OBSERVATIONAL AND NUMERICAL STUDY ON THE INFLUENCE OF LARGE-SCALE FLOW DIRECTION AND COASTLINE SHAPE ON SEA-BREEZE EVOLUTION

ROBERT C. GILLIAM, SETHU RAMAN* and DEV DUTTA S. NIYOGI

Department of Marine, Earth and Atmospheric Sciences, State Climate Office of North Carolina, North Carolina State University, Raleigh, NC 27695-7236, U.S.A.

Abstract. In this study radar, surface observations and numerical simulations are used to examine the inland penetration and intensity of the sea breeze during various large-scale flow regimes along the curved coastline of the Carolinas, U.S.A. The results clearly indicate that the flow direction relative to the curved coastline has a significant effect on the sea-breeze evolution. Overall, during northerly flow regimes along the curved North Carolina coast, observations and numerical simulations show that the sea-breeze front has a tendency to remain close to the south-facing coast. During these same flow regimes the front moves further inland relative to the east-facing coast. The sea-breeze front during westerly flow cases progressed further inland relative to the south coast and less so from the east-facing coastline. South-westerly flow allows the sea breeze to move inland from both coastlines but the coastal shape influence makes the inland penetration less from the easterly facing beaches. During periods of light onshore flow (south-east), the sea breeze moves considerable distances inland but is not discernable until later in the afternoon. The simulations indicated that the sea-breeze intensity is greatest (least) when the large-scale flow direction has an offshore (onshore) component. Model results indicate the existence of a strong front well inland in the late afternoon during light onshore flow. Also noted was that the simulated sea-breeze front develops earlier in the afternoon during offshore regimes and later in the day as the large-scale flow becomes more onshore. It is concluded that the coastline shape and coast-relative flow direction are important factors in determining how the sea-breeze circulation evolves spatially.

Keywords: Complex coastline, Doppler radar, Sea breeze, Sea-breeze circulations, Sea-breeze modelling, Synoptic-flow effects.

1. Introduction

The coastal region of North and South Carolina, U.S.A. (Figure 1) is an important socio-economic area, particularly during the warm season of May through September. Sea-breeze fronts regularly trigger severe weather events with dangerous lightning (Blanchard and Lopez, 1985), which directly influences various tourism and recreational activities, and hence the regional economy. The climatology of the region is affected by regular sea breezes; evidence has included signatures in the normal (climate) precipitation distribution (Moroz, 1967). Sea-breeze circulations are also important when considering pollutant transport and
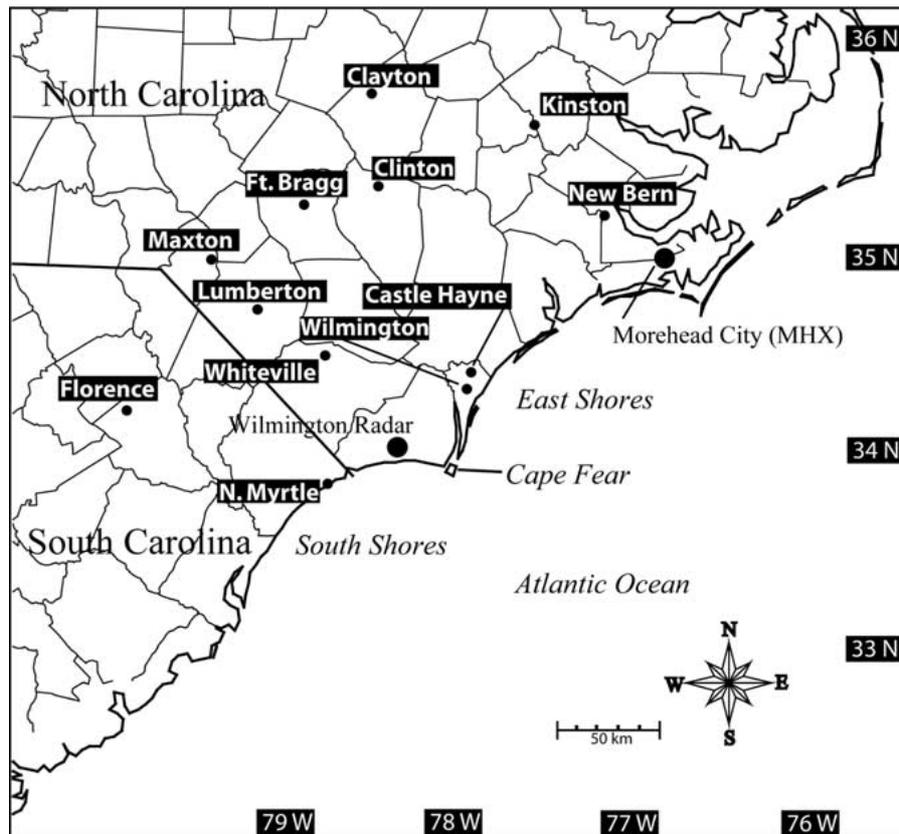
* E-mail: sethu_raman@ncsu.edu

Figure 1. Plan view of the study region showing the uniquely curved, south to east coastline of North and South Carolina. Also marked is the WSR-88D Doppler radar location near Wilmington, NC, surface observations locations and the rawinsonde upper air sounding location at Morehead City (MHX). The plan view also represents the domain covered by the 3D model case studies.

deposition near coastal areas (Lyons et al., 1973, 1976; Kitada and Ueda, 1989; Rhome et al., 2002). If an emergency situation such as a forest fire, bioterrorism or an accidental hazardous release of material occurs, the sea-breeze circulation needs to be explicitly considered (Simpson, 1994) by emergency management personnel.

Studies on sea-breeze evolution have highlighted that this mesoscale circulation is strongly influenced by regional scale features such as coastline configuration (McPherson, 1970), topography (Darby et al., 2002) and land use (Baker et al., 2001). Of these features, the curvature of the coastline (sometimes referred to as cusps) is the most prominent feature of the Carolina coastline. Hence, it is important to study the relationship between sea-breeze evolution and large-scale flow direction relative to the curved coastline in the Carolinas. To address this relationship, an observational analysis and numerical two-dimensional (2D) and three-dimensional (3D) simulations are performed.

Several observation-based and numerical studies have been conducted on the sea-breeze circulation to understand how large-scale flow modifies the inland penetration and the intensity of the sea-breeze front (e.g., Estoque, 1962; Pielke, 1974; Simpson, 1977; Abbs, 1986; Arritt, 1993). Results from these studies show that offshore synoptic flow strengthens the sea-breeze circulation, while onshore flow has the opposite effect. Using a 2D model, Arritt (1993) evaluated the maximum cross-shore wind component, vertical velocity, and inland penetration as a function of local time and ambient cross-shore wind strength. The study indicated that for a weak offshore flow the sea-breeze circulation was maximized near the coast and occurred just after the time of maximum insolation, between 1500 and 1700 local time (LT). Bechtold et al. (1991) evaluated the intensity of the sea breeze in terms of the maximum vertical velocity along the sea-breeze front and concluded that a 5 m s^{-1} offshore flow lead to the strongest sea-breeze circulation. Arritt (1993) had similar results but added that during offshore flow regimes where winds were stronger than 6 m s^{-1}, the sea-breeze circulation can still exist, but it remains offshore and never reaches the coast. During offshore flow situations where the flow is lighter (2-4 m s^{-1}), a moderate to strong sea-breeze front forms at the coastline in the early afternoon, preserving the horizontal temperature gradient between the sea-cooled air and sun-warmed land. Reible et al. (1993) indicated that this process maintains the density current identity, and hence strength of the sea breeze. This is because the low-level sea-cooled air never becomes modified by the warmer land, due to limited inland penetration of the sea breeze. For such situations, the sea-breeze front intensifies throughout the afternoon near the coastline, and then rapidly propagates inland in the late afternoon after it reaches maximum intensity (Physick, 1980; Plate, 1982).

Studies have shown that onshore synoptic flow forces a much different sea-breeze structure and evolution (Atkins and Wakimoto, 1997). Such sea-breeze fronts are less obvious since the sea-breeze low-level wind component is in the same direction as the larger-scale flow. However, Atkins and Wakimoto (1997) showed that both the low-level flow and the return flow aloft could be distinguished whenever the ambient or large-scale wind vector is subtracted from the observed wind. However, the sea breeze does not always form when the large-scale flow is directed onshore. Zong and Takle (1993) observed that an onshore flow greater than around 5 m s^{-1} completely eliminates any sea-breeze signature. Although sea-breeze fronts during light onshore flow situations are believed to be weak and ill-defined (Bechtold et al., 1991), its inland progression is much greater than during other flow regimes (Simpson, 1977; Reible et al., 1993; Buckley and Kurzeja, 1997).

Ambient flow parallel to the coastline presents an intermediate sea-breeze evolution relative to the onshore and offshore cases, although these cases are not well documented. However, a few studies have recognized these flow regimes, including that of Atkins and Wakimoto (1997) who showed that, in the afternoon during parallel flow situations, an increase and backing of the wind was evident inland but

the sea-breeze front was not obvious on Doppler radar until late afternoon. Helmis et al. (1995) identified a similar evolution along the Greek coast near Athens.

Considering recent and historic research on the sea breeze and its behaviour along curved coastlines during various flow regimes, several outstanding issues still exist. One of these issues is the effect of the unique coastline shape in the Carolinas on the sea-breeze evolution. McPherson (1970) was one of the first to examine the coastal shape effect on the sea breeze, but again the coastal shape was highly idealized and the numerical model simulations were somewhat limited. Numerical simulations by Baker et al. (2001) indicated that Cape features in Florida strongly influence the sea breeze but questions still arise as to how the uniqueness of the cusps along the coastline affect these processes in the Carolinas. Atkins and Wakimoto (1997) studied the Florida sea breeze during a variety of flow regimes but the coast considered was relatively linear. Zong and Takle (1993) noted that the complex coastline features around Cape Canaveral influenced convergence patterns of the sea-breeze front in that region but their study area has much less curvature as compared to the Carolina cusps. Arritt (1989) studied the effect of different coastline shapes on the sea breeze but the shapes were idealized and different synoptic flow directions were not modelled. Abbs (1986) examined, in detail, observations and numerical simulations over a range of synoptic flows for a complicated bay area in southern Australia, but nearby mountains were a complicating factor. These are not present near the Carolina coast.

The above studies provide a firm base for our hypothesis that the curvilinear coastline of the region and the large-scale flow significantly alters the Carolina sea breeze. Our hypothesis testing involves two tasks. The first, explores the sea-breeze evolution using an idealized 2D numerical model. The focus of the 2D analysis is on how various flow directions relative to the coast influence the sea breeze while the wind speed remains constant (i.e. with changes in the wind vector). The second part of the study examines observed cases along the Carolina coast, where the synoptic flow was from different directions in order to gain more understanding of the coastline curvature and synoptic flow on the sea breeze. The analysis includes Doppler radar observations and surface data, which are used to investigate variations in the sea-breeze circulation that are mainly a result of the synoptic flow pattern. Additionally, these observations are compared with results from 3D model simulations as well as the 2D simulations to provide more information on these interactions.

Accordingly, Section 2 describes the modeling set-up and the experimental study undertaken. The observations used for validating the model results are also discussed in this section. In Section 3, the results of the 2D and 3D simulations are presented. In particular, attention is given to four observed cases for which the large-scale flow varied along different directions relative to the coast. A summary and the results of the study are presented in Section 4.

2. Experimental Design

2.1. NUMERICAL MODEL CONFIGURATIONS

Numerical model simulations of the atmosphere are an important part of the hypothesis testing of this investigation. Two-dimensional simulations were used to first develop a simple relationship between the wind direction and inland penetration and intensity of the sea breeze. Then, three-dimensional simulations were used to examine the variations in sea-breeze characteristics along the complex coastline of the Carolinas. The Advanced Regional Prediction System (ARPS), a non-hydrostatic, fully compressible, primitive equation model (Xue et al., 1995), was used for both the 2D and 3D numerical experiments. Tables I and II summarize the basic model configurations used in this research.

The 2D domain consisted of 55×4 horizontal grid cells with a grid spacing of 5 km, split with 170 km (34 grid cells) defined as land and 105 km (21 grid cells) as water. Sixty vertical grid points are stretched from the surface to 16 km with 25 grid layers below 3 km (Table I). For all 2D simulations the model was initialized at 0700 LT, corresponding approximately to sunrise, then integrated 15 hours until 2200 LT. The set-up of the 3D model simulations was nearly identical except that the vertical grid was limited to 30 grid points, with 15 layers below 3 km (Table II). Additionally, the 3D model simulations were initialized one hour earlier (0600 LT), since 3D cases possibly need more time to attain equilibrium as compared to 2D configurations.

The lateral and top boundary conditions were prescribed as zero gradient and the bottom boundary was a no-slip rigid wall in both sets of simulations. Turbulence was parameterized using a 1.5-order TKE turbulence closure scheme (Sun and Chang, 1986). Moist processes were considered using Lin et al. (1983) microphysics parameterization. A cumulus parameterization (Kain and Fritsch, 1993) was used in both 2D and 3D simulations. Radiation physics was incorporated using a atmospheric radiation transfer parameterization; this includes solutions for both shortwave (Chou, 1990, 1992) and longwave (Chou and Suarez, 1994) processes. Surface fluxes were calculated using stability dependent surface drag coefficients. Additional details related to these parameterizations and the model formulation can be found in the ARPS Users Guide version 4.0 or Xue et al. (1995), or Xue et al. (2000, 2001).

ARPS contains a coupled two-layer soil-vegetation model (Noilhan and Planton, 1989) that simulates interaction between the surface and atmospheric boundary layer. This soil-vegetation model requires surface properties such as soil type (texture), surface roughness, leaf area index, and vegetation fraction. Although these surface variables do show significant spatial variability at times, they were prescribed homogeneous, including only the regionally dominant features: loamy sand, roughness length of 0.1 m, a leaf area index of 2, and a fractional vegetation cover of 0.4 (Table III). This was done primarily to eliminate small-scale effects

TABLE I

Specifications for the two-dimensional ARPS simulations.

Centre location	34.0° N and 78.0° W
Horizontal grid cells	55 × 4 (nx × ny)
Horizontal grid spacing (km)	5
Vertical grid spacing (m) below 3 km	5, 19, 40, 68, 106, 152, 208, 273, 350, 437, 536, 648, 772, 909, 1060, 1226, 1406, 1601, 1812, 2028, 2281, 2539, 2815
Start time LT)	0700
End time (LT)	2200
Large time step (explicit) (sec)	10
Small time step (implicit) (sec)	5

Parameterizations: 1.5 TKE turbulence closure, Kain and Fritsch cumulus, atmospheric radiation transfer, Noilhan and Planton soil model.

TABLE II

Specifications for the three-dimensional ARPS simulations.

Centre location	34.0° N and 78° W
Horizontal grid cells	90 × 90 (ny × ny)
Horizontal grid spacing (km)	5
Vertical grid spacing (m) below 3 km	10, 40, 95, 170, 280, 420, 600, 800, 1050, 1340, 1675, 2050, 2475, 2950
Start time (LT)	0600
End time (LT)	2200
Large time step (explicit) (sec)	10
Small time step (implicit) (sec)	5

Parameterizations: 1.5 TKE turbulence closure, Kain and Fritsch cumulus, atmospheric radiation transfer, Noilhan and Planton soil model.

of land use variations that were noticed in more realistic test simulations, so the sea-breeze circulations only respond to the influence of coastline shape.

In addition to the surface boundary specification, an atmospheric sounding of potential temperature, specific humidity, wind speed and direction was used to initialize the model. In the 2D simulations, a typical warm-season potential temperature and moisture profile was used from the rawinsonde station located in Morehead City (MHX), and is shown in Figure 2. The single sounding model initialization option assumes horizontally homogeneous temperature, moisture and wind speed profiles. This initialization was the same for each of the 2D simulations; only the wind direction was varied (Table IV). The wind direction intervals were 30° for all quadrants except between 180 and 270° where simulations were

TABLE III

Surface properties of the two and three-dimensional ARPS simulations.

Soil type	Loamy sand
Roughness (m)	0.10
Leaf-area index	2
Vegetation fraction	0.40

TABLE IV

Initial conditions for the two-dimensional ARPS simulations.

Initial meteorological profiles	
Wind speed (m s^{-1})	2
Wind directions	30°, 60°, 90°, 120°, 150°, 180°, 195°, 210°, 225°, 240°, 255°, 270°, 300°, 330°, 360°
Potential temperature and moisture	See Figure 2
Initial soil properties	
Soil temperature (surface and deep)	295 K
Soil moisture (surface and deep)	0.20 kg kg^{-1}
Sea surface temperature	295 K

performed every 15°. This was done to provide more details around the average summertime wind direction, which is from the south-west. In the 3D cases, the morning (1200 UTC or 0700 LST) soundings from MHX (wind, temperature and moisture) were used in a similar manner to initialize the model. Figure 3 shows the skew-T diagram of the sounding used for each of the 3D cases.

Table IV provides the prescribed initial soil temperature, soil moisture and sea surface temperatures for the 2D simulations. The initial soil temperature and air temperature were set the same (295 K), and the soil moisture was set to a typical value of 0.20 kg kg^{-1} for the region, based on soil moisture observations and analysis in North Carolina such as Sims et al. (2002). Sea-surface temperature was homogeneous and set equal to the initial soil temperature (295 K). The 3D simulations were initialized with an average sea-surface temperature value of the near shore waters, which was estimated from AVHRR satellite imagery. The initial soil temperature was set equal to the observed sea-surface temperature.
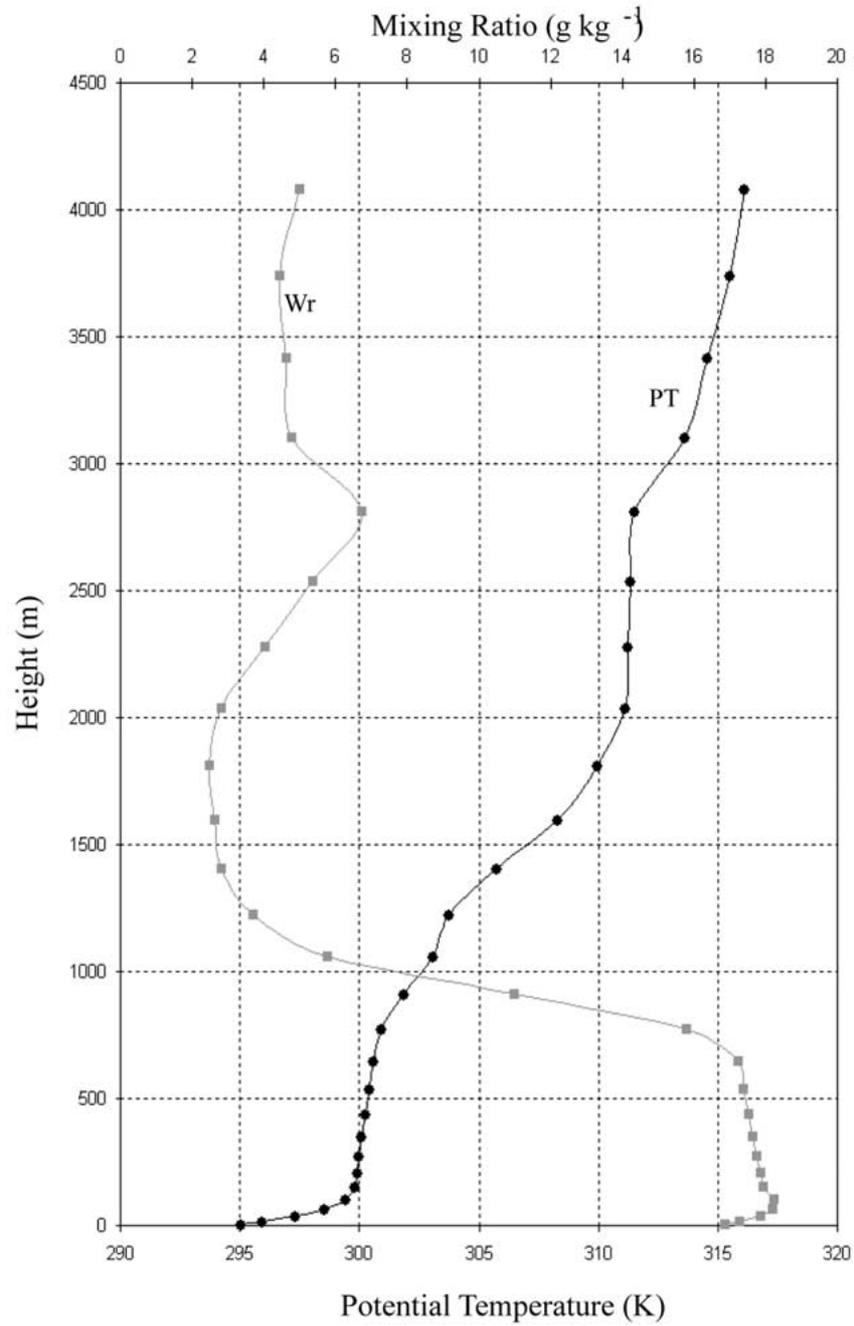
Figure 2. Potential temperature (PT) and mixing ratio (Wr) profiles used in the series of 2D simulations as initial conditions starting at 0700 LT. These data were taken from a typical summertime sounding at Morehead City in the morning (0700 LT).
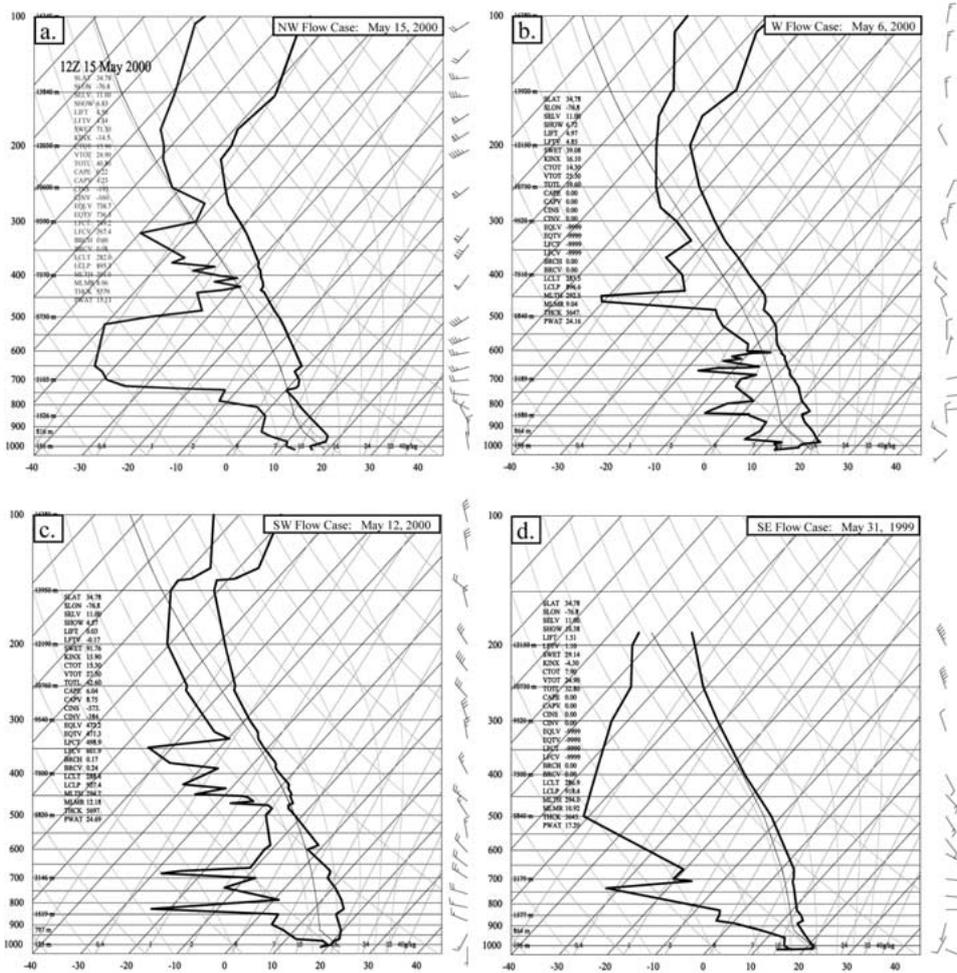
Figure 3. Upper-air soundings at 0800 LT (1200 UTC) from Morehead City, N.C. The profiles were used to initialise the 3D ARPS simulations for the different synoptic flow cases. (a) North-westerly flow on May 15, 2000, (b) westerly flow on May 06, 2000, (c) south-south-westerly flow on May 12, 2002, and (d) south-easterly flow on May 31, 1999.

2.2. OBSERVATIONS

WSR-88D Doppler radar has the ability to detect many types of convergence zones. Sea-breeze fronts are seen as a thin line of enhanced radar reflectivity, a result of mostly insects and debris (Rayleigh Scattering) trapped in the updraft along the front. After reviewing a number of frontal events, cases were chosen for several different large-scale flow regimes that typically occur in North Carolina during the warm season. Four cases are presented: North-north-west (NNW), west (W), south-south-west (S-SW), and south-east (SE) synoptic flow scenarios. The large-scale flow direction was estimated by examining the sea-level pressure gradient

pattern and the near-surface wind flow from the 1200 UTC (0800 LT) Eta Data Assimilation System (EDAS) analysis.

For each of the cases, Doppler radar images were collected from the Wilmington, North Carolina National Weather Service (NWS) radar at the time that the sea breeze reached full intensity. These images are used to approximate the inland penetration of the sea-breeze front relative to the coastline. In order to increase the accuracy of the inland penetration estimates, the data were geo-referenced and analyzed using ArcView GIS software. The aim was to accurately quantify the sea-breeze front location relative to the coastline. Two inland penetrations were recorded: (i) Perpendicular distance from the east-facing coast to the closest location of the sea-breeze front and similarly (ii) for the south-facing coast.

Additional observations used in the analysis are based on the NWS Automated Surface Observing System (ASOS) and North Carolina Environmental and Climate Observing Network (NC ECONet) (Niyogi et al., 1998).

3. Results

3.1. TWO-DIMENSIONAL MODEL SIMULATIONS

The sea-breeze circulation was examined on an hourly basis for each 2D simulation. The inland penetration distance and maximum vertical velocity were identified and plotted with respect to the local time and the prescribed initial flow direction. The results are presented in the context of a coast-relative flow coordinate system; Figure 4 illustrates this frame of reference in which land is to the left and water to the right. Offshore flow is defined as a wind direction of zero degrees, while 180 or −180° represent onshore flow. A negative angle indicates a backing or counter-clockwise flow relative to offshore flow (e.g., from westerly to southerly) and a positive angle indicates the flow is clockwise relative to offshore flow (e.g., from westerly to northerly flow). Figure 5 presents the nomogram of inland penetration distance with respect to local time and the coast-relative flow direction. The data indicate that when the large-scale flow direction is parallel to shore, from the south (−90°), the inland penetration of the sea breeze is approximately 20 km at 1300 LT as marked by location (**a1**) in Figure 4. Note that, these effects are for a 3D coastline where the synoptic flow direction is assumed uniform, and the coast-relative flow varies according to the coastline curvature. For instance, along the southern North Carolina coast around Wilmington (Figure 1), the shoreline curves from facing south to facing east, yielding a 90° change in coastline orientation. This 90° change directly corresponds to a 90° variation in coast-relative flow. For instance, a westerly mean wind flow results in an offshore wind along the east-facing coast, while along the south-facing coast the flow is parallel to shore. Referring to Figure 5, it is clear that such a change in coast-relative flow results in different inland penetration distances at any particular time.
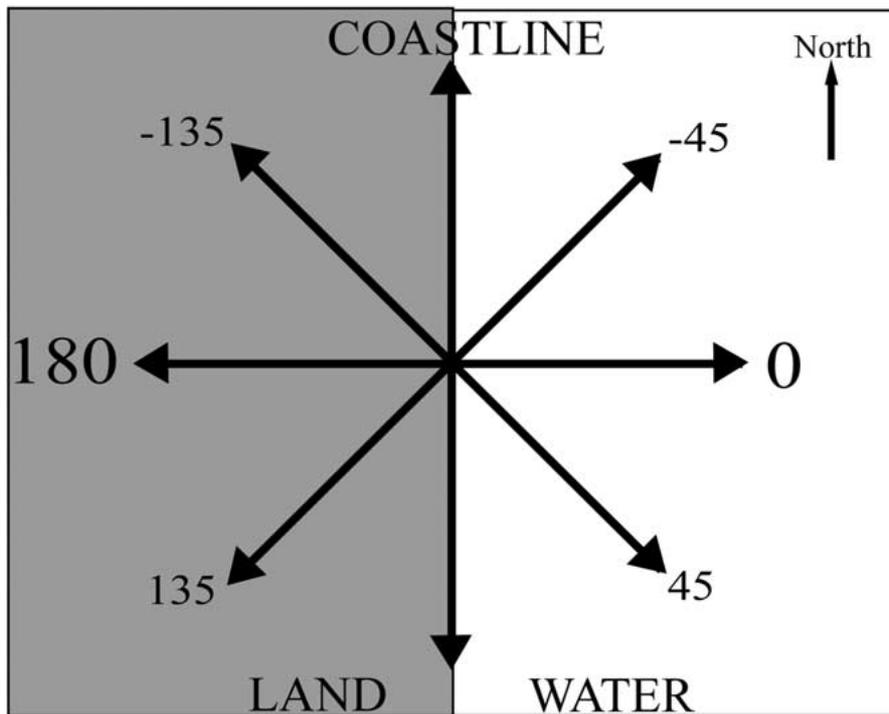
Figure 4. Coast relative coordinate system used in the inland penetration and intensity nomograms derived from the 2D ARPS simulations. The arrows indicate the wind flow direction relative to the north-south coastline.

In general the 2D simulation results shown in Figure 5 are consistent with past sea-breeze studies (Plate, 1982; Arritt, 1993; Atkins and Wakimoto, 1997). That is, offshore winds restrict the sea-breeze front from propagating inland, while onshore flow causes the front to advance further inland. The simulation results in Figure 5 indicate that at 1700 LT, the sea-breeze front would be located 20, 40 and 70 km inland for offshore, alongshore and onshore synoptic flow regimes, respectively. In the Carolinas, where there is a 90° curvature in the coastline orientation, the nomogram indicates that there would be a variation in the sea-breeze inland penetration that is a result of the coast-relative large-scale flow. An example of the variability is when the region experiences a south-west (−45°) flow. The coast-relative wind direction ranges from approximately −45° (east-facing beaches) to −135° (south-facing beaches). Accordingly, the simulated inland penetration distances at 1700 LT corresponding to this flow are 28 km (**b1**) from the east-facing coastline and 60 km (**b2**) from the south-facing coast. Conversely, a large-scale wind direction from the north-west (+45°) would result in a less dramatic variation in inland penetration according to Figure 5. If this were the case, the coast-relative flow would be −45 along the south-facing coast and +45° along the east coast. The corresponding inland penetration in Figure 5 at 1700 LT relative to both the east
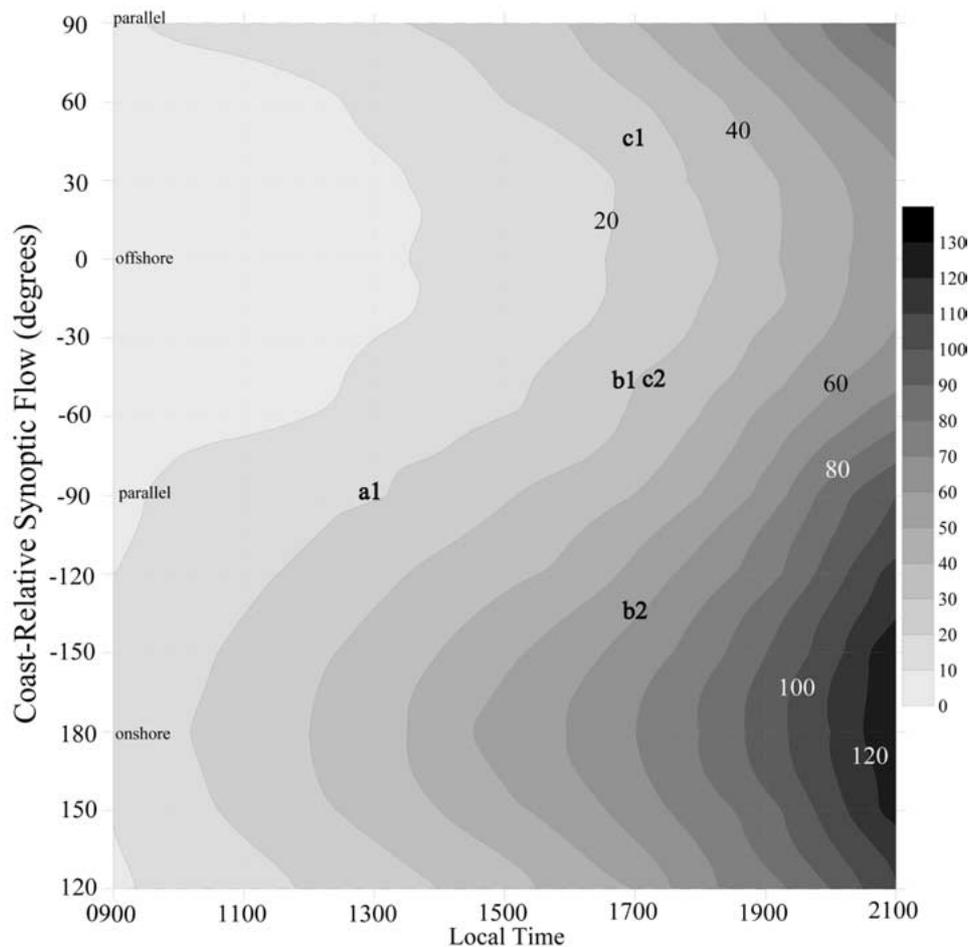
Figure 5. The simulated inland penetration distance (km) of the sea-breeze front as a function of local time and coast relative large-scale flow direction. The numbers and shading correspond to the inland penetration contours. Labels a1, b1, b2, c1, and c2 correspond to the inland penetration distances for the scenarios discussed in the results. Data were extracted from the series of two-dimensional model simulations. The coast-relative synoptic flow direction follow the modified coordinate system explained by Figure 4.

(**c1**) and south (**c2**) facing coasts is about the same, around 30 km. Arritt (1993) presented 2D simulations that suggested that during a 2 m s^{-1} offshore flow the inland penetration would be about 60 km .

An examination of the gradient of inland penetration distance with respect to local time in Figure 6 provides information regarding the propagation speed of the front. For offshore flow regimes (0°) the sea-breeze front remains within 10 km of the coastline through early afternoon (1300 LT) at which point the front begins to quickly move inland. This is consistent with surface observations during offshore
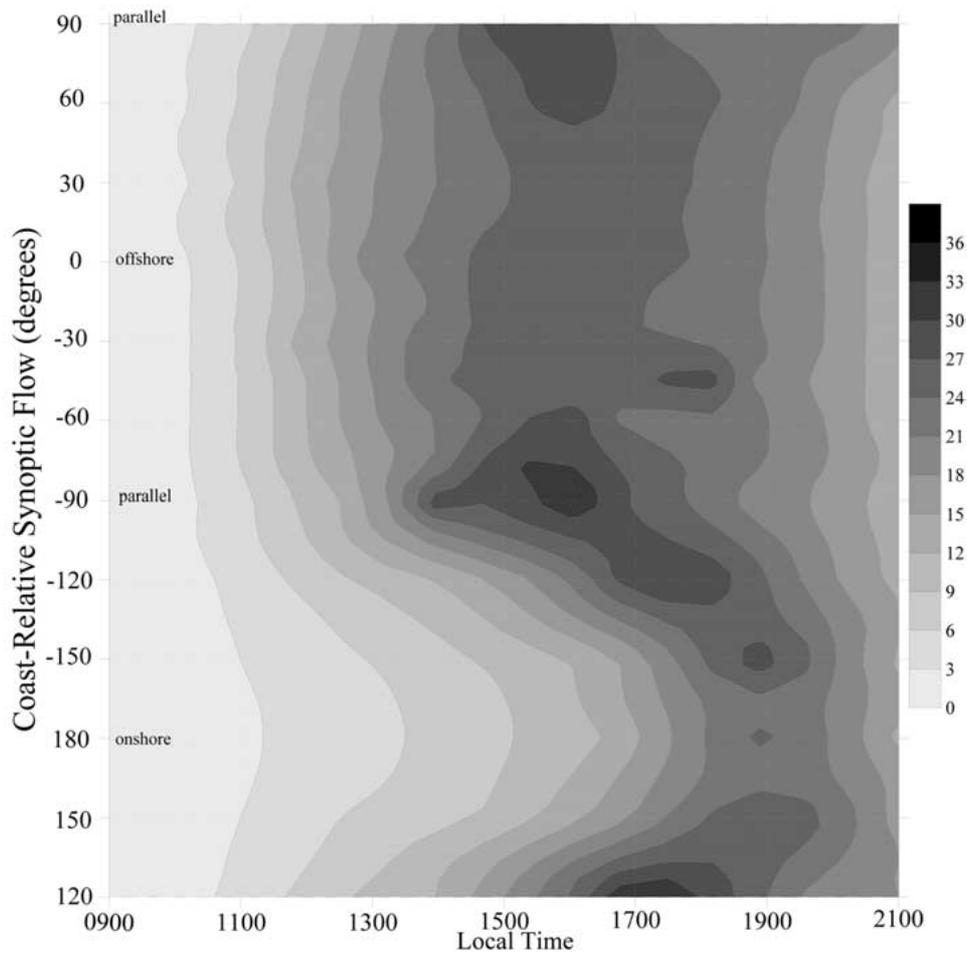
Figure 6. The simulated sea-breeze frontal intensity (cm s^{-1}) as a function of local time and coast relative large-scale flow direction. The shaded contours correspond to the vertical velocity at 800 m. Data were extracted from the series of two-dimensional model simulations. The coast-relative synoptic flow direction follows the modified coordinate system explained by Figure 4.

flow cases noted by Rieble et al. (1993). For southerly flow parallel to the shore ($-90°$) the frontal propagation speed is much larger in the early afternoon and increases rapidly through the evening. The time series for onshore flow, as expected, shows that the front moves inland more quickly as compared to all other flow regimes.

Figure 6 shows the time evolution of the maximum vertical velocity of the sea-breeze front with respect to the large-scale flow direction. For scenarios where the large-scale flow has an offshore component, the sea-breeze frontal intensity is the greatest. For the offshore flow regimes, the frontal intensity (shown by the vertical velocity) reaches a maximum in the mid-afternoon (1600 LT), which agrees with

the numerical study of Arritt (1993) as well as several observational studies (Atkins and Wakimoto, 1997; Simpson et al., 1977). The simulation results indicate that the maximum vertical velocity is slightly greater for parallel flow as compared to offshore flow. This anomalous result is not completely understood as most studies show a stronger front during offshore flow situations. One explanation however, is that the maximum vertical velocity was obtained at the same level in all simulations. Studies have shown that the depth of the sea-breeze front is different between offshore, parallel and onshore flow situations so this would imply that the level of maximum upward motion also varies. For example, Arritt (1993) indicated that the inflow layer was about 650 m for light offshore flow (2 m s^{-1}) and increased as the offshore flow strength decreased.

For onshore flow, Figure 6 indicates that the front reaches maximum intensity relatively later in the day (1800–2000 LT) with a similar intensity as offshore flow regimes. This is not completely supported by previous research, but may be partially explained by the fact that the initial wind speed in these experiments was low (2 m s^{-1}). This may imply that during light synoptic flow, the strength of the sea-breeze front is similar between onshore and offshore flow regimes. Furthermore, the plot shows that it is mainly the time of the maximum intensity that varies for different light flow regimes, not as much the strength. Some support is provided by Simpson (1977), who observed a strengthening late day sea-breeze front (2140 LT) that propagated significant distances (around 100 km) inland. Buckley et al. (1997) also observed and modeled well-defined inland sea-breeze fronts in the early evening over South Carolina. Additionally, radar observations presented below do support a strong inland sea-breeze front just before sunset during light onshore flow. Thus, this model result appears to be physically possible, though of limited occurrence.

3.2. CASE STUDIES OF THE CAROLINA SEA BREEZE

Sea-breeze cases were collected in the spring of 1999 and 2000 and grouped based upon the large-scale flow pattern. Four cases that represented typical flow situations in the Carolinas were selected for this study. Frequently weak cold fronts propagate through the region in the late spring and early summer, followed by brief periods of northerly winds. Thus, a north-west flow (May 15, 2000) case was chosen and will be the first to be examined. Climatologically, the predominant flow direction during the warm season is from the south-west. Two cases were chosen to represent the normal flow pattern across the Carolinas, a westerly flow (May 6, 2000) and a south-south-westerly flow (May 12, 2000) case. The fourth case (south-east flow: May 31, 1999) represents a light south-easterly flow pattern that occurs often when pressure increases off the east coast of the U.S. and a deep tropical flow is present across the southern states. In the following analysis, the Doppler radar images of the sea-breeze fronts are examined along with surface observations and

the EDAS analysis, and then compared to the quasi-idealized 3D ARPS simulation for coastline shaped effects.

3.2.1. *Case 1: North-Westerly Flow*

The first case occurred on May 15, 2000. A surface high-pressure system was strengthening from the west at 0800 LT (1200 UTC) after the passage of a weak cool front on the previous day. In Figure 7a, the EDAS analysis indicates a 5–7 m s^{-1} near-surface northerly wind over the coastal region of the Carolinas. A low-pressure system off the North Carolina coast quickly moved north-east, resulting in diminishing wind speeds as a high pressure system moved just north of the area by 2000 LT (0000 UTC). Surface observations indicated a maximum daytime 2-m temperature of 298 K near the coast and 300 K well inland. The satellite determined sea-surface temperature was approximately 295 K.

The Doppler radar base reflectivity for this case at 1700 LT is shown in Figure 8a. The sea-breeze front is well-defined by the radar as a thin line of higher reflectivity. The northerly synoptic flow has a noticeable influence on the inland penetration of the front, and the front is closer to the south-facing coastline where the northerly wind is directed offshore. Conversely, relative to the east-facing coastline the synoptic flow is parallel to shore. Less opposing winds allow the sea-breeze front to penetrate further inland relative to the east coast. Using GIS software to determine geographic distance measurements, the observed maximum sea-breeze penetration is 50 km from the east-facing coast while the front is about half that distance from the southern facing coast (25 km). The 2D estimated inland distances (Figure 5) are not in fair agreement with the observations, suggesting that at 1700 LT a sea-breeze front penetrates inland approximately 23 km during offshore flow and 38 km during along shore flow. Additionally, results shown in Figure 6 indicate that at approximately 1700 LT the sea breeze reaches its maximum intensity, during both offshore and parallel shore flow. This numerical result corresponds well with the intense narrow region of high reflectivity in the Doppler imagery. Subsequent radar images reveal that the front weakens quickly after this time.

The simulated vertical velocities at 800 m from the ARPS 3D model simulation along with the simulated 10-m wind vectors and surface wind observations are shown in Figure 9a. The 5 m s^{-1} easterly wind reported by the surface observations, near the Wilmington coast confirms that the sea breeze has penetrated inland. However, there is poor agreement between the 3D simulation and the observational data. Likewise, there is poor agreement between the 3D simulation and the 2D nomogram. The 3D model simulated the front location offshore through the afternoon, never allowing inland penetration. Overland, 10-m winds are on the order of 5 to 7 m s^{-1} from the north-west, while the surface observations indicate that the wind is light and variable across the region. The lack of agreement between the 3D simulation and observations can be explained as follows. First of all the assumption stated in the 3D simulations was that the initial wind distribution is horizontally homogeneous and the boundary conditions are zero gradient. This
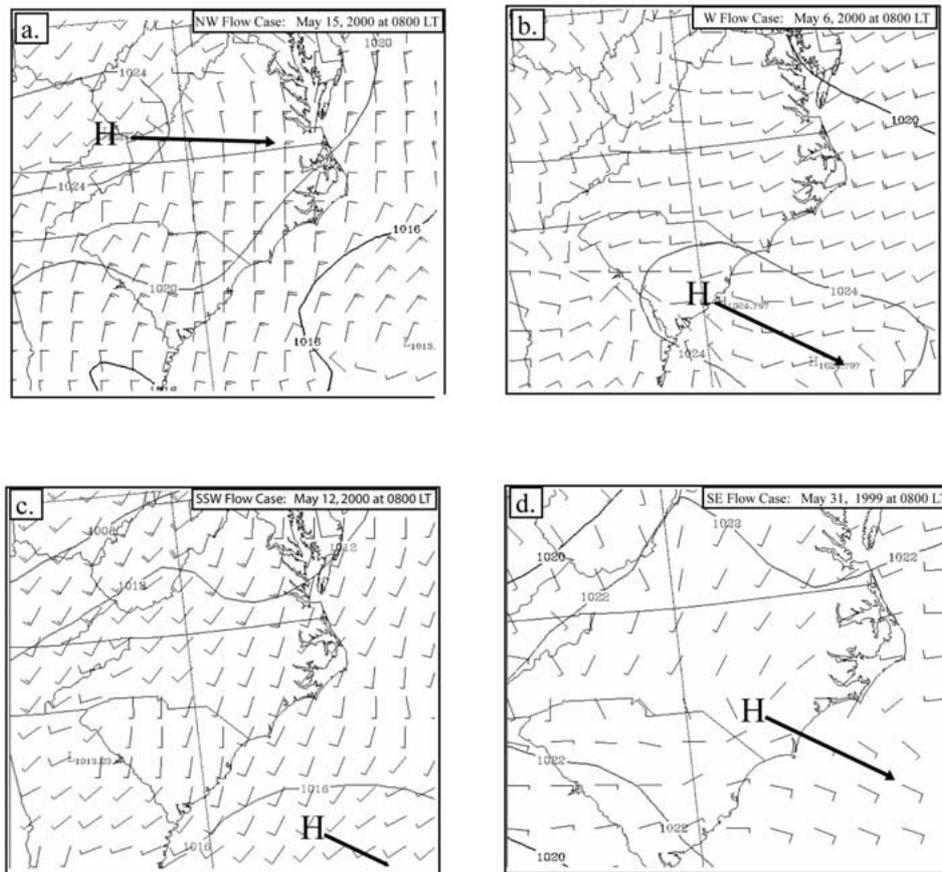
Figure 7. Eta Data Assimilation System (EDAS) analysis maps showing sea-level pressure and near surface wind barbs (knots) at 0800 LT (1200 UTC) for the four sea-breeze case studies. 'H' and arrow represents the movement of the surface high-pressure cell through the day. The date/time corresponds to the soundings show in Figure 3, and each represents a different flow regime. Note that 1 knot $\equiv 0.514$ m s^{-1}.

does not allow the large-scale flow to vary through the day, as actually occurred when a high pressure system moved just north of the region in the afternoon. The initial simulated flow from the north-west continued through the day with the same strength as was initially prescribed by the Morehead City sounding. From earlier studies, it has been shown that moderate (5 to 7 m s^{-1}) offshore winds will maintain the sea breeze on or just off the coast and not allow significant inland penetration, so with the given flow and assumptions of the model simulation, the model results are not considered false. Frizzola and Fisher (1963) estimated approximate off-shore flow strength of 4 to 8 m s^{-1} would prevent the Long Island, N.Y. sea breeze from moving inland. Watts (1955) indicated that a large land-water temperature difference (11 K) is needed to overcome an 8 m s^{-1} offshore wind, a temperature
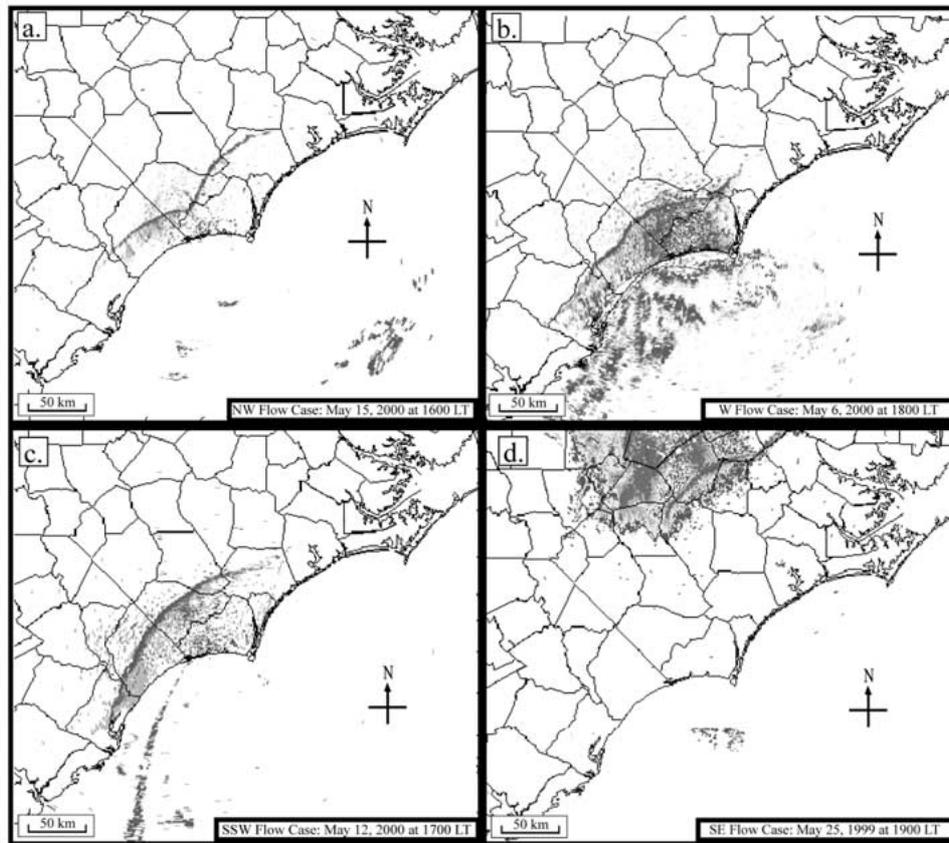
Figure 8. WSR-88D Doppler radar images in clear air mode of the Carolina sea-breeze front. The sea-breeze front is seen as the thin line of high radar reflectivity. The radar site for Panel a, b and c is near Wilmington (refer to Figure 1). The RaleighDurham radar was used to detect the inland sea breeze in Panel d.

difference not realized in this case. More recently, Arritt (1993) found that the sea breeze does not move inland when the opposing flow is greater than 5 to 7 m s^{-1}.

Some important features of the 3D sea-breeze simulation can be deduced. Mainly, there are stronger areas of upward motion offshore of the Cape areas and relatively weaker upward motion in the centre of the Bay areas when the sea-breeze front is forced to remain offshore. The Cape areas act to focus low-level convergence as the sea-breeze wind component backs towards the Cape. Conversely, the subsidence zone offshore is greatest in the centre of the Bays, while less adjacent to the Capes. It is noticed that the wind offshore of Cape Fear is from the southwest, while the wind along the coast and just inland is north-west. Not only is there directional convergence, but speed convergence is present too. Just offshore from the sea-breeze front, the wind is almost calm while inland it is 5 to 7 m s^{-1}. Pett and Tag (1984) suggested this calm zone is most prominent when an offshore large-
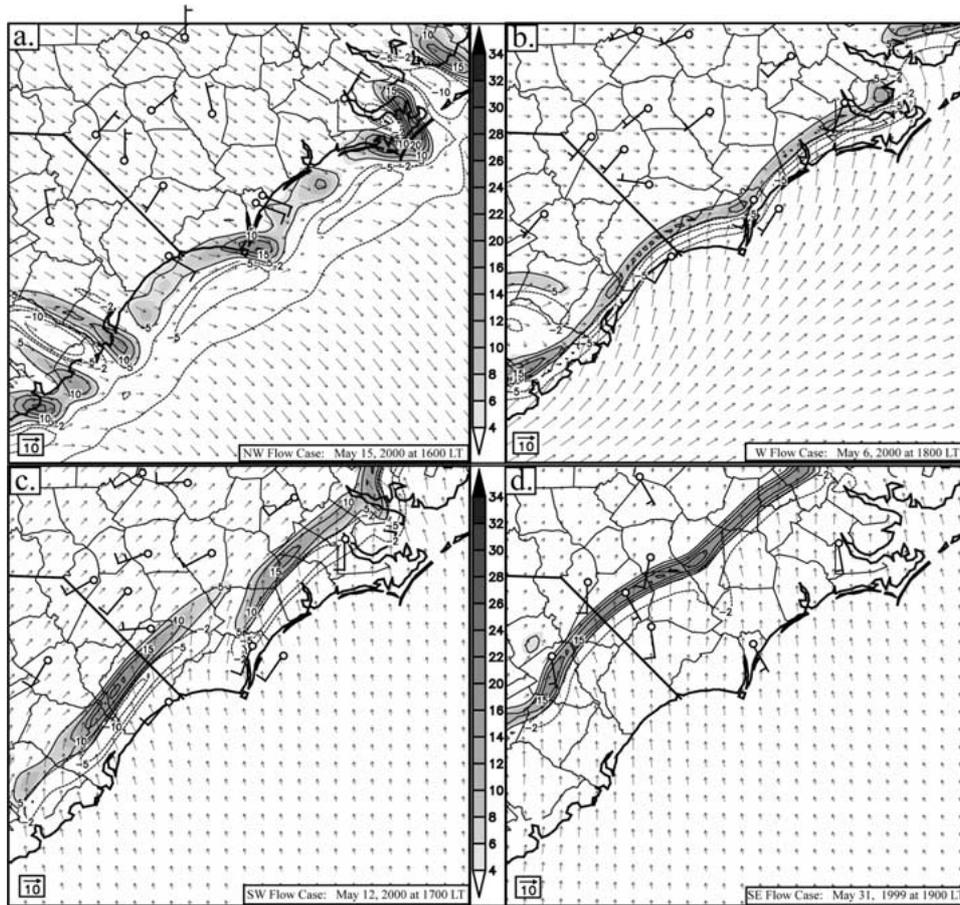
Figure 9. Contours of the simulated vertical velocity (cm s^{-1}) at 800 m corresponding to the radar images in Figure 8. Also shown are the simulated 10-m wind vectors (m s^{-1}) and surface wind observations with the standard wind barb notation (knots).

scale flow is nearly balanced by the sea onshore sea-breeze components. This type of wind distribution was also discussed in the modelling work of Arritt (1989) and confirmed by various satellite and observational analysis (Neumann, 1951; Lyons and Olsson, 1973). These variations can be of importance in marine forecasting and possibly pollution transport issues.

3.2.2. *Case 2: Westerly Flow*

The westerly flow case (Case 2) analyzed in this section, occurred on May 6, 2000; EDAS surface analysis (Figure 7b) estimates a westerly surface wind speed of 5 m s^{-1}. Sea-level pressure analysis show an area of high pressure to the south of the region, over the coastal area of South Carolina at 0800 LT (1200 UTC). In Figure 7b, the arrow indicates the south-eastward movement of the high-pressure cell

through the daytime. Surface observations along the coast reported temperatures reaching a maximum daytime value of 302 K, while inland temperatures reached 304 K. Satellite imagery of the sea surface indicated that the sea temperatures were around 295 K. Warm days, as in this case in the late spring when water temperatures are still relatively cool, lead to strong sea-breeze formation in the Carolinas.

Figure 8b shows the late afternoon sea-breeze front at 1800 LT as observed by Doppler radar. During westerly flow episodes, the offshore wind component is greatest along the east-facing beaches of the Carolinas. On the other hand, along the south-facing coast the large-scale flow is parallel to shore. Accordingly, inland penetration is greatest relative to the south-facing shore and least relative to the east-facing coast. At this time the sea breeze has penetrated approximately 45 km inland from the south beach and 30 km inland from the east beach. The 2D model results indicate that the penetration is around 30 km inland from the east coast and 50 km from the south. As in the previous case, the intensity of the sea-breeze front in Figure 6 correlates well with the intense front that is detected by Doppler radar.

The 3D simulation for the westerly case is shown in Figure 9b. The simulated vertical motion at 800 m indicates a well-defined sea-breeze front with southerly winds along the coast within the sea-breeze circulation and westerly winds inland. Surface observations near the coast are in good agreement with the southerly sea-breeze flow, however, further inland the simulated winds are more westerly than the observations. Through the day, the high pressure cell to the south of the region moved south-eastward, resulting is a more southerly flow across the area, which as discussed in the previous case, not represented by the 3D model simulation. However, the frontal position and strength reveal a coastline shape influence on the sea-breeze evolution that is supported by the radar observations. The simulated front, and the observed front, are further inland relative to the south-facing coast. Additionally, an area of higher upward motion exists just north of the Cape, where the coastline curvature induces more low-level wind convergence (Baker et al., 2001). This is the intersection location of the two distinct sea-breeze fronts, one originating from the east-facing coast and one from the south-facing coast. The simulated front is several kilometres closer to both the southern and eastern coasts than the Doppler observations, and even more so than the 2D simulation predictions.

3.2.3. *Case 3: South-South-Westerly Flow*

Case 3 corresponds to a sea-breeze event that occurred during a south-south-west large-scale flow on May 12, 2000. EDAS analysis in Figure 7c shows the general south-south-westerly flow with a wind speed of 5 m s^{-1} near the surface. This case represents the most frequent synoptic flow pattern in the Carolinas during the late spring and summer seasons, as the persistent Bermuda High usually remains stationary off the south-east coast of the U.S. The satellite data (not shown) suggest that the sea-surface temperature was around 295 K, while surface observations reported coastal air temperatures reaching 304 K in the early afternoon and inland

temperatures reaching 308 K in the mid-afternoon. This temperature difference, on the order of 10 K between the land and sea, has the potential to induce a strong sea-breeze circulation.

Consistent with the synoptic conditions, at 1700 LT, the Wilmington Doppler radar (Figure 8c) data indicated the development of a very intense sea-breeze front that moved well inland. A south-south-westerly synoptic flow has a slight onshore component along the south facing beaches while there is a small offshore component relative to the east-facing coast. GIS analysis indicates that the Doppler observed sea-breeze front penetrated further inland (65 km) relative to the south coast while it remained slightly closer (30 km) to the east-facing beaches. The sea-breeze front simulated by the simplified 2D model suggested that the sea-breeze front would be approximately 65–70 km inland (Figure 5) at this time, if the flow was onshore, and about 35–40 km if the flow was nearly parallel to the shore, with just a slight offshore component.

Results from the 3D model simulation are also in agreement with the observations. Figure 9c shows the inland position of the simulated sea-breeze front. The location is in agreement with the Doppler radar front in Figure 8c. Further, the intensity of the observed and modelled fronts are also similar. The southernmost portion of the observed front in Figure 8c appears to be more intense, since the radar reflectivity is greater. The simulated vertical motion in Figure 9c is strongest in the same area where the large-scale flow relative to the coastline has the greatest offshore component. Another similar region of strong upward motion is simulated adjacent to the eastern facing coast, just north of Wilmington. The Wilmington radar did not have the range to sense the sea-breeze front in this area and the Morehead City radar data were not available, but radar data from the Wilmington site taken several hours earlier do reveal a separated sea-breeze-front like structure stretching from the Cape Fear river to the north and east as shown in the numerical simulation.

The surface observations are also in agreement with the simulated wind field, specifically the observation at New Bern that indicates a southerly wind while Kinston (locations shown in Figure 1) to the north-west is reporting a south-west wind. These observations further confirm that the sea-breeze front is in a similar location as simulated in the 3D simulation. One anomalous observation is at North Myrtle Beach, which reported a south-west wind although the radar clearly shows the sea-breeze front is well inland. This may have been a reporting error as observations around this time indicate a southerly wind.

Another interesting feature of this case was the presence of a dual sea-breeze structure in the model simulation. This feature has not been extensively reported in earlier sea-breeze studies. Consideration of the coast-relative flow provides a possible explanation for this phenomenon. Along the southern coast the flow is almost entirely onshore; this coast-relative flow orientation forces the sea-breeze front well inland and, consistent with the 2D cases, results in a very weak front at 1700 LT. As the shore curves to face a eastward direction, the coast-relative flow

becomes parallel to the coast. Again, consistent with the 2D nomogram shown in Figure 5, when the flow is parallel to shore the front intensity significantly increases relative to the onshore flow scenario and time of day. The 3D simulation results show these two fronts to eventually intersect and combine later in the day.

The agreement in this case between the 2D and 3D simulations, and observations, are likely the result of the more persistent synoptic flow pattern relative to the previous cases where the pattern was evolving throughout the day. This case further illustrates that during an approximate stationary synoptic situation, which occurs often during the warm season, the simple 2D nomogram of inland penetration distance and intensity agrees with 3D simulations and could be a simple, efficient tool in predicting the sea breeze evolution.

3.2.4. *Case 4: South-Easterly Flow*

Case 4 presents the final case (May 31, 1999) where the synoptic flow is onshore over the entire coastal area. The EDAS surface analysis at 0800 LT (Figure 7d) shows a weak pressure gradient corresponding to a light east-south-east flow over the coastal Carolina region. Surface observations from a coastal site recorded maximum temperature around 300 K while inland temperature rose to 303 K. Sea-surface temperature data indicate water temperatures around 298 K.

Figure 8d shows the location of the sea-breeze front well inland at approximately 1900 LT at its maximum intensity. This is consistent with past studies (Simpson, 1977; Buckley et al., 1997), which have shown during light onshore flow that the sea breeze can penetrate a considerable distance inland and not strengthen until later in the day (Atkins and Wakimoto, 1997). In this case the front was not detected by radar until 1900 LT, after it had penetrated approximately 120 km from the coastline. A similar but slightly less inland penetration was simulated by the 2D model, which predicted that the sea breeze would penetrate about 95 km inland by 1900 LT during onshore flow. Additionally, the 2D simulations agree well with the frontal intensity reaching a maximum just after 1900 LT, as shown by the simulated vertical velocity in Figure 6. The observed sea-breeze front continued to propagate for several more hours, penetrating nearly 140 km inland, and then quickly weakened after sunset.

The 3D model simulation for this onshore case is presented in Figure 9d. The plotted surface observations are in agreement with the model simulations, with surface observations indicating light southerly winds. The modelled sea-breeze front is well inland, and in close proximity to the observed Doppler radar front. The simulated front is characterized as a strong narrow region of upward motion consistent with the radar observations. The vertical motion is stronger that the previous two cases, and is consistent with the analysis presented by Buckley et al. (1997) over South Carolina.

Another feature to note is the area of stronger upward motion in some regions along the sea-breeze front, which appears to directly result from the coastline curvature. These stronger frontal locations would likely be focus mechanisms for

convective activity in an unstable atmosphere. Additionally, these late day inland fronts are important features to consider in operational forecasting, as they often trigger convection or interact with existing thunderstorm outflow boundaries to initiate new convective complexes (Koch and Ray, 1997).

3.2.5. *Average Sea-Breeze Intensity*

From the sea-breeze fronts observed by Doppler radar, surface observations and model analysis, it is evident that the coastline shape and synoptic flow relative to the coastline have a dominant influence on sea-breeze evolution. The vertical velocity at 800 m averaged over the entire simulated sea-breeze cycle is shown for each case in Figure 10; Figure 10a corresponds to the north-west flow case. This average vertical velocity indicates the areas around the Capes experience the strongest portion of the sea-breeze front, while areas in the centre of the Bay experience the weakest front further offshore. Additionally, the vertical velocity is stronger compared to the other cases. It has been observed and confirmed through discussion with local mariners and weather observers that the area around, the appropriately named, Cape Fear is prone to thunderstorms. Baker et al. (2002) support this idea with simulations that show convex coastline areas cause stronger convergence and more thunderstorm activity.

Figure 10b shows the vertical velocities, similar to Figure 10a, except for the westerly flow case. The average vertical velocity distribution is as expected, stronger close to the east-facing coast and further inland from the south-facing coast. A similar area of stronger, upward motion exists just north of Cape Fear, where curvature increases convergence. Similar areas exist at other locations along the Carolina coast where the curvature abruptly changes, particularly along the peninsular areas around Morehead City (refer to Figure 1).

The spatial distribution of the average vertical motion for the south-south-west case is shown in Figure 10c. A striking pattern is observed, specifically that during southerly flow regimes where the front adjacent and just north of the easterly facing beaches corresponds to the strongest portion of the sea-breeze front. This frontal intensity pattern reveals a direct influence of coastline shape and highlights areas along the front that are more likely to initiate deep convection. It is evident again that the coast-relative synoptic flow is a major factor in the sea-breeze variations.

The distribution of averaged vertical velocity at 800 m for the onshore case is shown in Figure 10d. The average vertical motion is less than the previous cases because the front moves farther inland over the same period of time. There is, however, a pattern in the vertical motion average along the sea-breeze front influenced by the coastline shape. The vertical motion is greatest just inland from the Cape areas, in the direction of the south-east flow. As with the other cases, identification of this pattern is useful in predicting the most likely areas of thunderstorm initiation.
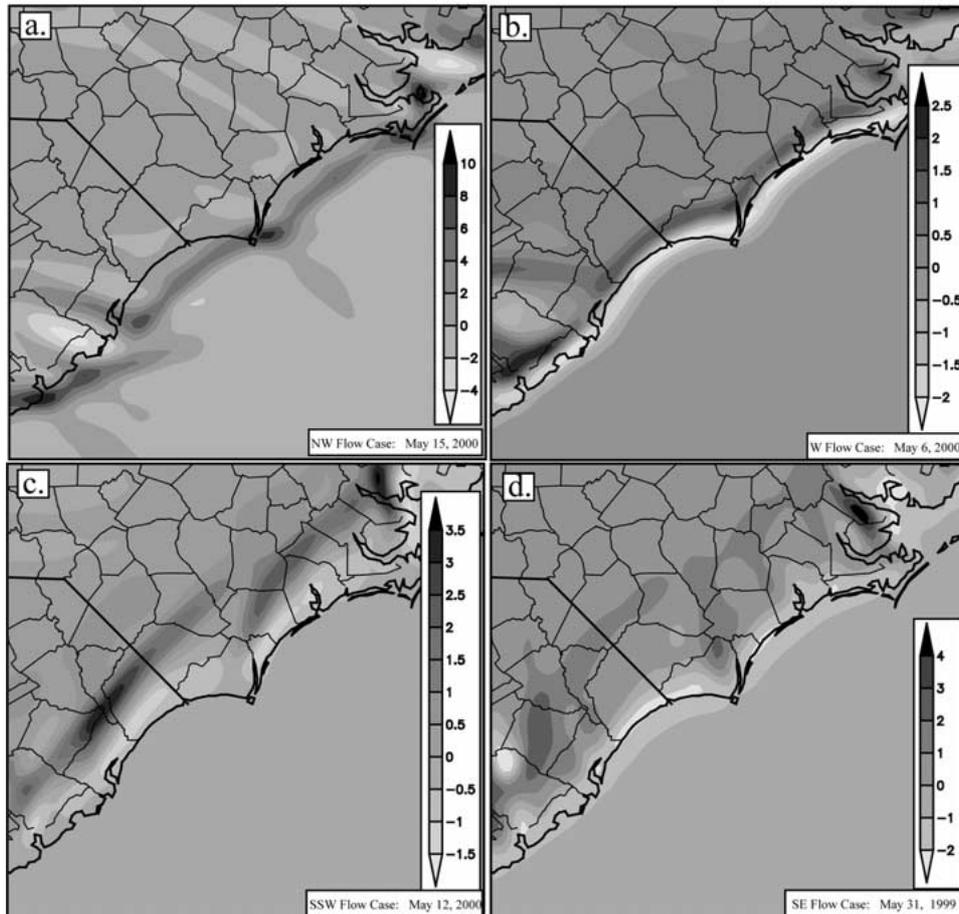
Figure 10. Average vertical velocity (cm s^{-1}) at 800 m between 0600 LST and 2300 LST for each of the four sea-breeze cases.

4. Summary and Conclusions

The sea breeze is a nearly daily occurrence in the coastal area of the Carolinas for a large portion of the year, and both direct and indirectly affects the population. Because of this, it is critical to more fully understand the evolution of this important weather system. A series of 2D and 3D simulations were performed and compared with observations of the sea-breeze front location and intensity along the Carolina coast. The main objective was to gain insight into how the large-scale flow affects the sea-breeze evolution along a curved coastline.

This study has shown that there is a pronounced relationship between coastline shape, synoptic flow and the sea-breeze evolution in the Carolinas. Sea-breeze fronts along curved coastlines do not move inland at equal speed, nor do they have the same intensity, because the synoptic scale flow relative to the coastline varies.

North-west flow in the Carolinas limits the sea breeze from propagating inland along the coast. The front will usually remain close to the coast and the frontal intensity is the greatest compared to the other flow regimes, especially when the opposing flow is around 4 to 6 m s^{-1}. These fronts form early in the afternoon and diminish before sunset. The front that forms adjacent to the east-facing coast moves further inland than the front that forms along the south-facing coast. If the opposing flow is sufficiently strong as shown in the 3D model case, the entire sea-breeze circulation can be forced offshore from the southerly facing shores while remaining closer to the coast along the easterly facing beaches. Curvature of the coastline causes stronger areas of upward motion near the Cape areas and weaker vertical motion over the Bays.

Westerly flow induces a strong front, propagating inland from the southern facing beaches while being held closer to the coast along the easterly beaches. These fronts also form early in the afternoon reaching a maximum intensity just after the time of maximum solar radiation, then diminishing before sunset as they advance inland. As with the north-westerly flow case, the cusp areas like Cape Fear and around Morehead City have stronger sea-breeze convergence because of the coastal shape.

South to south-westerly flow allows a moderate front to develop and move a significant distance inland as compared to the more offshore flow regimes. The front moves further inland from the south-facing coast while remaining closer to the east-facing coast. These fronts form around the time of maximum solar insolation and may persist until sunset. A dual sea-breeze frontal structure was simulated for this flow direction consistent with the observations. This structure is a direct effect of the coast-relative large-scale flow, and the strongest part of the sea-breeze front was just inland from the east-facing beaches.

Onshore light wind flow regimes (north-easterly to south-easterly) can produce intense sea-breeze fronts. These fronts propagate furthest inland – on the order of 100 km or more. Sea-breeze fronts that form during these flow regimes typically do so in the early evening when turbulent fluxes decline, and can last briefly after sunset. There is some evidence in the model simulations that the Cape areas cause slightly more convergence along the inland sea-breeze front.

These results can potentially be related to other coastlines with similar features. The nomogram of inland penetration distance is a potential tool that can be used to quickly estimate the location of the sea breeze at any point during the day.

References

Abbs, D. J.: 1986, 'Sea-Breeze Interaction along a Curved Coastline in Southern Australia: Observations and Numerical Modeling Study', *Mon. Wea. Rev*. **114**, 831–848.

Arritt, R. W.: 1989, 'Numerical Modeling of the Offshore Extent of Sea Breeze', *Quart. J. Roy. Meteorol. Soc.* **115**, 547–570.

Arritt, R. W.: 1993, 'Effects of Large Scale Flow on Characteristic Features of the Sea Breeze', *J. Appl. Meteorol.* **32**, 116–125.

Atkins, N. T. and Wakimoto: 1997, 'Influences of the Synoptic-Scale Flow on Sea Breezes Observed during CAPE', *Mon. Wea. Rev.* **125**, 2112–2130.

Baker, R. D., Lynn, B. H., Boone, A., Tao, W., and Simpson, J.: 2001, 'Influence of Soil Moisture, Coastline Curvature, and Land-Breeze Circulations on Sea-Breeze-Initiated Precipitation', *J. Hydrometeorol.* **2**, 193–211.

Bechtold, P., Pinty, J. P., and Mascart, P.: 1991, 'A Numerical Investigation of the Influence of Large-Scale Winds on Sea-Breeze and Inland-Breeze Type Circulations', *J. Appl. Meteorol.* **30**, 1268–1279.

Blanchard, D. O. and Lopez, R. E.: 1985, 'Spatial Patterns of Convection in South Florida', *Mon. Wea. Rev.* **113**, 1282–1299.

Buckley, R. L. and Kurzeja, R. J.: 1997, 'An Observational and Numerical Study of the Nocturnal Sea breeze. Part I: Structure and Circulation', *J. Appl. Meteorol.* **36**, 1577–1598.

Chou, M. D.: 1990, 'Parameterization for the Absorption of Solar Radiation by O_2 and CO_2 with Application to Climate Studies', *J. Climate* **3**, 209–217.

Chou, M. D.: 1992, 'A Solar Radiation Model for Climate Studies', *J. Atmos. Sci.* **49**, 762–772.

Chou, M. D. and Suarez, M. J.: 1994, *An Efficient Thermal Infrared Radiation Parameterization for Use in General Circulation Models*, NASA Tech Memo 104606, 85 pp.

Darby, L. S., Banta, R. M., and Pielke, R. A.: 2002, 'Comparisons between Mesoscale Model Terrain Sensitivity Studies and Doppler Lidar Measurements of the Sea Breeze at Monterey Bay', *Mon. Wea. Rev.* **12**, 2813–2838.

Estoque, M. A.: 1962, 'The Sea Breeze as a Function of the Prevailing Synoptic Situation', *J. Atmos. Sci.* **19**, 244–250.

Frissola, J. A. and Fisher, E. L.: 1963, 'A Series of Sea Breeze Observations in the New York City Area', *J. Appl. Meteorol.* **24**, 722–739.

Helmis, C. G., Papadopoulos, K. H., Kalogiros, J. A., Soilemes, A. T., and Asimakopoulos, D. N.: 1995, 'Influence of Background Flow on Evolution of Saronic Gulf Sea Breeze', *Atmos. Environ.* **29**, 3689–3701.

Kain, J. S. and Fritsch, J. M.: 1993, 'Convective Parameterization for Mesoscale Models: The Kain–Fritsch Scheme. The Representation of Cumulus Convection in Numerical Models', *Meteorol. Monogr., Amer. Meteorol. Soc.* 165–170.

Kitada, T. and Ueda, H.: 1989, 'Pollutant Dispersion and Land/Sea Breeze Circulations', in *Encyclopedia of Environmental Control Technology*, Gulf Publishing Company, pp. 583–630.

Koch, S. E. and Ray, C. A.: 1997, 'Mesoanalysis of Summertime Convergence Zones in Central and Eastern North Carolina', *Wea. Forecast.* **12**, 56–77.

Lin, Y. L., Farley, R. D., and Orville, H. D.: 1983, 'Bulk Parameterization of Snow Field in a Cloud Model', *J. Clim. Appl. Meteorol.* **22**, 1065–1092.

Lyons, W. A. and Cole, H. S.: 1976, 'Photochemical Oxidant Transport. Mesoscale Lake Breezes and Synoptic Scale Aspects', *J. Appl. Meteorol.* **15**, 733–743.

Lyons, W. A. and Olsson, L. E.: 1973, 'Detailed Mesometeorological Studies of Air Pollution Dispersion in the Chicago Lake Breeze', *Mon. Wea. Rev.* **101**, 387–403.

McPherson, R. D.: 1970, 'A Numerical Study of the Effect of a Coastal Irregularity on the Sea Breeze', *J. Appl. Meteorol.* **9**, 767–777.

Moroz, W. J. and Hewson, E. W.: 1966, 'The Mesoscale Interaction of a Lake Breeze and Low-Level Outflow from a Thunderstorm', *J. Appl. Meteorol.* **5**, 148–155.

Neumann, J.: 1951, 'Land Breezes and Nocturnal Thunderstorms', *J. Meteorol.* **8**, 60–67.

Niyogi, D., Raman, S., and Perry, K.: 1998, 'NC ECO Net: Towards an Integrated Climate and Environmental Observation Network for North Carolina', in *23rd Conference on Agricultural and Forest Meteorology, Albuquerque, New Mexico*, November 25, 1998, pp. 227–231.

Noilhan, J. and Planton, S.: 1989, 'A Simple Parameterization of Land Surface Processes for Meteorological Models', *Mon. Wea. Rev.* **117**, 536–549.

Pett, R. W. and Tag, P. M.: 1984, 'The Sea-Breeze Induced Coastal Calm Zone as Revealed by Satellite Data and Simulated by a Numerical Model', *Mon. Wea. Rev.* **112**, 1226–1233.

Physick, W. L.: 1980, 'Numerical Experiments on the Inland Penetration of the Sea Breeze', *Quart. J. Roy. Meteorol. Soc.* **106**, 735–746.

Pielke, R. A.: 1974, 'A Three-Dimensional Numerical Model of the Sea Breezes over South Florida', *Mon. Wea. Rev.* **102**, 115–139.

Plate, E. J.: 1982, *Engineering Meteorology*, Elsevier Scientific, Amsterdam, New York, 288 pp.

Reible, D., Simpson, J. E., and Linden, P. F.: 1993, 'The Sea Breeze and Gravity Current Frontogenesis', *Quart. J. Roy. Meteorol. Soc.* **119**, 1–16.

Rhome, J., Niyogi, D., and Raman, S.: 2003, 'Assessing Seasonal Transport and Deposition of Agricultural Emissions in Eastern North Carolina, USA', *Pure Appl. Geophys.* **160**, 117–141.

Simpson, J. E.: 1994, *Sea-Breeze and Local Winds*, Cambridge University Press, Cambridge, 234 pp.

Simpson, J. E., Mansfield, D. A., and Milford, J. R.: 1977, 'Inland Penetration of Sea-Breeze fronts', *Quart. J. Roy. Meteorol. Soc.* **103**, 47–76.

Sims, A., Niyogi, D., and Raman, S.: 2002, 'Use of Drought Indices for Developing Soil Moisture Information: A North Carolina Case Study', *Geophys. Res. Lett.* **29**, 241–244.

Sun, W. Y. and Chang, C. Z.: 1986, Diffusion Model for a Convective Layer. Part I: Numerical Simulation of Convective Boundary Layer', *J. Clim. Appl. Meteorol.* **25**, 1445–1453.

Watts, A. J.: 1955, 'Sea Breeze at Thorney Island', *Meteorol. Mag.* **84**, 42–48.

Xue, M.: 1995, *Advanced Regional Prediction System (ARPS) Users Guide, Version 4.0*, Centre for Analysis and Prediction of Storms, 380 pp.

Xue, M., Droegemeier, K. K., and Wong, V.: 2000, 'The Advanced Regional Prediction System (ARPS) – A Multi-Scale Nonhydrostatic Atmospheric Simulation and Prediction Tool. Part I: Model Dynamics and Verification', *Meteorol. Atmos. Phys.* **75**, 161–193.

Xue, M., Droegemeier, K. K., Wong, V., Shapiro, A., Brewster, K., Carr, F., Weber, D., Liu, Y., and Wang, D.: 2001, 'The Advanced Regional Prediction System (ARPS) – A Multi-Scale Nonhydrostatic Atmospheric Simulation and Prediction Tool. Part II: Model Physics and Applications', *Meteorol. Atmos. Phys.* **76**, 143–165.

Zhong, S. and Takle, E. S.: 1993, 'The Effects of Large-Scale Winds on the Sea-Land-Breeze Circulations in an Area of Complex Coastal Heating', *J. Appl. Meteorol.* **32**, 1181–1195.